Negative refraction without absorption via quantum coherence

Ai-Ping Fang,[1] Wenchao Ge,[2] Meng Wang,[1] Fu-li Li,[1] and M. Suhail Zubairy[2]

[1]*Shaanxi Province Key Laboratory of Quantum Information and Quantum Optoelectronic Devices and Department of Applied Physics, School of Science, Xi'an Jiaotong University, Xi'an 710049, People's Republic of China*

[2]*Institute for Quantum Science and Engineering (IQSE) and Department of Physics and Astronomy, Texas A&M University, College Station, Texas 77843, USA*

(Received 2 December 2015; published 18 February 2016)

Negative refraction of a probe field is studied in a dense gas consisting of cascade-type four-level atoms. By coupling the magnetic component of the probe field to a Λ scheme with initially prepared coherence in the two lower levels, strong negative permeability with minimal absorption can be obtained. The permittivity of the gas to the electric component of the probe field can be made negative by taking into account the local field effect of the dense atoms. Strong negative refraction with zero absorption can be achieved in a wide range of parameters in our scheme. A possible experimental realization is also discussed.

DOI: 10.1103/PhysRevA.93.023822

I. INTRODUCTION

The linear response of materials to electromagnetic waves is determined by two frequency-dependent parameters: electric permittivity (ε) and magnetic permeability (μ). Veselago [1] showed that a material with both $\varepsilon < 0$ and $\mu < 0$ can reveal a negative index of refraction. Such negative refraction materials promise many surprising and counterintuitive features such as the reversals of both Doppler shift and Cerenkov radiation [1], negative Goos-Hänchen shift [2], amplification of evanescent waves [3], and subwavelength focusing [4]. More interestingly, it may become possible to make a "perfect lens" in which imaging resolution is not limited by the diffraction limit by use of a slab of negative refractive materials [5]. Until now, most of the approaches to the realization of negative refractive index materials are limited to artificial structures such as metamaterials [6–12] and photonic crystal structures [13–15]. In such negative refractive materials, negative refraction commonly suffers from resonant absorption especially towards higher frequencies, which limits many possible applications [5,16]. On the other hand, requiring the periodical array of electric and magnetic resonators may lead to the extreme difficulty of manufacturing two- or three -dimensional materials with negative refractive index in the optical regime [17–19].

Atomic gases can macroscopically extend in all spatial directions and an atom has naturally both electric and magnetic transitions between different states. Thus, atomic gases are naturally three-dimensional materials with both electric and magnetic susceptabilities. Recently, an alternative approach of the realization of negative refraction in dense atomic gases have been proposed [20]. In an atomic gas, the magnetic susceptibility is usually smaller than the electric susceptibility by four orders of amplitude. Thommen and Mandel [21] proposed to make a significant change of the permeability from a magnetic moment induced by coupled electric transitions. More recently, many atomic schemes [22–25] have been studied to show negative refraction via electromagnetically induced chirality [22]. More importantly, suppressed absorption as well as negative refraction in atomic gases has been suggested [25–29] by means of electromagnetic induced transparency [30] and gain mechanisims.

In this paper, we propose an idea to achieve negative refraction without absorption in a dense atomic gas via atomic coherence [31]. In our scheme, the electric component and the magnetic component of a probe field interact with different atomic transitions, respectively. Initial atomic coherence is prepared to stimulate strong negative permeability with minimal absorption, therefore the scheme does not require an external strong driving field to induce chirality in the medium. Negative permittivity is obtained by taking into account the local field effect due to the dense atoms. First, we derive from the master equation the steady-state solution of the response of the atoms in the presence of a weak probe field. Then we give explicit expressions of both the real part and the imaginary part of the refractive index due to the local field effect of the dense atoms and the interaction between the atom gas and the probe field. Finally, we study for a wide range of parameters to show the feasibility of negative refraction with zero absorption in our scheme.

This paper is organized as follows. In Sec. II, we present the model and derive the analytical results for negative refraction. In Sec. III, we study the numerical results for negative refraction by varying different parameters for the purpose of realistic implementation and we show negative refraction with figure of merit (FOM) $\gg 1$, where FOM is defined as $|\mathrm{Re}[n]|/|\mathrm{Im}[n]|$ to quantify the performance of our scheme. In Sec. IV, we draw a conclusion of the model studied in this paper.

II. THE MODEL

A. The scheme

In our scheme, we consider the atoms with four cascade levels involved as shown in Fig. 1. The ground state consists of a level doublet $|a\rangle$ and $|b\rangle$ which have the same parity. The level $|c\rangle$ has same parity with the levels $|a\rangle$ and $|b\rangle$ and the transition from $|c\rangle$ to $|a\rangle$ ($|b\rangle$) is electric-dipole forbidden but magnetic-dipole allowed with the magnetic-dipole moment μ_{ca} (μ_{cb}). The level $|d\rangle$ has the opposite parity with the level $|c\rangle$ and the transition from $|d\rangle$ to $|c\rangle$ is electric-dipole allowed with the electric-dipole moment d_{dc}. The energy of each state $|i\rangle$ is $\hbar\omega_i (i = a,b,c,d)$ and the corresponding decay rates of the levels to other external levels are $\gamma_a,\gamma_b,\gamma_c,\gamma_d$, respectively.

The transition $|d\rangle$ to $|c\rangle$ is coupled by the electric component of a probe field with the frequency ω_p. The transitions $|c\rangle$

 ©2016 American Physical Society

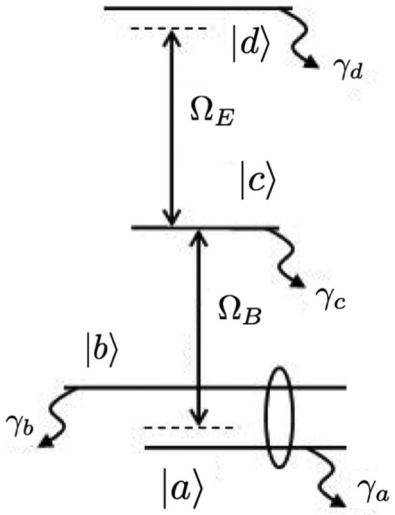

FIG. 1. Atomic level configuration.

to $|a\rangle$ and $|c\rangle$ to $|b\rangle$ are both coupled by the magnetic component of the probe field. The probe field is detuned from the transitions $|c\rangle \rightarrow |a\rangle, |c\rangle \rightarrow |b\rangle$ and $|d\rangle \rightarrow |c\rangle$ by $\Delta_{ca} = \omega_c - \omega_a - \omega_p, \Delta_{cb} = \omega_c - \omega_b - \omega_p$, and $\Delta_{dc} = \omega_d - \omega_c - \omega_p$, respectively.

We assume that the atoms are initially prepared at a rate r_p in a coherent superposition of states, which is described by the density matrix

$$\rho(0) = \rho_{dd}^{(0)}|d\rangle\langle d| + \rho_{cc}^{(0)}|c\rangle\langle c| + \rho_{bb}^{(0)}|b\rangle\langle b| + \rho_{aa}^{(0)}|a\rangle\langle a| + \rho_{ab}^{(0)}|a\rangle\langle b| + \rho_{ba}^{(0)}|b\rangle\langle a|. \quad (1)$$

Here the off-diagonal elements $\rho_{ab}^{(0)}$ and $\rho_{ba}^{(0)}$ represent the atomic coherence that can lead to the quantum interference between two transition paths from the ground state doublet to the excited state $|c\rangle$ and the cancellation of photon absorption [31]. The preparation of the coherence states can be accomplished by coherent pulse excitation [32], Raman-induced coherence [33], and adiabatic population conversion using two coherent pulses with time delay [34].

Suppose that the electric and the magnetic component of the probe field are linearly polarized along x axis and y axis, respectively, and have the form $\mathbf{E}(t) = \xi_E \cos(\omega_P t)\mathbf{e}_x, \mathbf{B}(t) = \xi_B \cos(\omega_P t)\mathbf{e}_y$, where ξ_E and ξ_B are the amplitudes of the two components. In the interaction picture with dipole approximation and the rotating-wave approximation, the Hamiltonian of the system reads

$$H = \hbar\Delta_{cd}|d\rangle\langle d| - \hbar\Delta_{ca}|a\rangle\langle a| - \hbar\Delta_{cb}|b\rangle\langle b| - \frac{\hbar}{2}(\Omega_E e^{i\varphi_3}|d\rangle\langle c| + \Omega_{B2}e^{i\varphi_2}|c\rangle\langle b| + \Omega_{B1}e^{i\varphi_1}|c\rangle\langle a| + \text{H.c.}), \quad (2)$$

where $\Omega_{B1} = |\mu_{ca}|\xi_B/\hbar, \Omega_{B2} = |\mu_{cb}|\xi_B/\hbar$ and $\Omega_E = |d_{dc}|\xi_E/\hbar$ are magnitudes of Rabi frequencies of the probe field for different atomic transitions. φ_i are the corresponding phases of the electric and magnetic dipole moments defined as $\mu_{ca} = |\mu_{ca}|e^{i\varphi_1}, \mu_{cb} = |\mu_{cb}|e^{i\varphi_2}$ and $d_{dc} = |d_{dc}|e^{i\varphi_3}$.

B. The steady-state solution

The equation of motion for the density matrix of the atoms takes the following form:

$$\frac{\partial\rho}{\partial t} = -\frac{i}{\hbar}[H,\rho] - \frac{1}{2}\{\Gamma,\rho\} + r_p\rho^{(0)}, \quad (3)$$

where the decay matrix Γ is defined by $\langle i|\Gamma|j\rangle = \delta_{ij}\gamma_i$. In our scheme, the populations in the excited states ($|c\rangle$, $|d\rangle$) are very small and therefore the collective decay is not important. If the probe field strength is weak compared to the atomic decay, then it is sufficient only to consider the linear response of the atom to the probe field. Therefore, the off-diagonal matrix elements of the density matrix for the atoms are kept to the lowest order in either the electric amplitude ξ_E or the magnetic amplitude ξ_B and the diagonal matrix elements are kept to the zeroth order. Under this approximation, the steady-state solution of the relevant density matrix elements is given as

$$\begin{aligned}
\rho_{ca} &= -\frac{i}{2}\frac{\Omega_{B1}e^{i\varphi_1}}{(i\Delta_{ca}+\gamma_{ca})}\left[\frac{r_p}{\gamma_c}\rho_{cc}^{(0)} - \frac{r_p}{\gamma_a}\rho_{aa}^{(0)}\right] + \frac{i}{2}\frac{\Omega_{B2}e^{i\varphi_2}}{(i\Delta_{ca}+\gamma_{ca})}\frac{r_p\rho_{ba}^{(0)}}{(i\omega_{ba}+\gamma_{ba})} \\
\rho_{cb} &= -\frac{i}{2}\frac{\Omega_{B2}e^{i\varphi_2}}{(i\Delta_{cb}+\gamma_{cb})}\left[\frac{r_p}{\gamma_c}\rho_{cc}^{(0)} - \frac{r_p}{\gamma_b}\rho_{bb}^{(0)}\right] + \frac{i}{2}\frac{\Omega_{B1}e^{i\varphi_1}}{(i\Delta_{cb}+\gamma_{cb})}\frac{r_p\rho_{ab}^{(0)}}{(-i\omega_{ba}+\gamma_{ba})}, \\
\rho_{dc} &= -\frac{i}{2}\frac{\Omega_E e^{i\varphi_3}}{(i\Delta_{dc}+\gamma_{dc})}\left[\frac{r_p}{\gamma_d}\rho_{dd}^{(0)} - \frac{r_p}{\gamma_c}\rho_{cc}^{(0)}\right], \\
\rho_{aa} &= \frac{r_p}{\gamma_a}\rho_{aa}^{(0)}, \quad \rho_{bb} = \frac{r_p}{\gamma_b}\rho_{bb}^{(0)}, \quad \rho_{cc} = \frac{r_p}{\gamma_c}\rho_{cc}^{(0)}, \\
\rho_{dd} &= \frac{r_p}{\gamma_d}\rho_{dd}^{(0)}, \quad \rho_{ab} = \frac{r_p}{(-i\omega_{ba}+\gamma_{ba})}\rho_{ab}^{(0)}.
\end{aligned} \quad (4)$$

Here the off-diagonal elements ρ_{ca} and ρ_{cb} are due to the overall effect of the probe field and the initial atomic coherence. The full master equations of the density matrix elements are given in Appendix and the results of the steady-state solution are derived under the weak probe field approximation. Since $\Omega_E \gg \Omega_{B1}, \Omega_{B2}$, we consider $\Omega_E \sim 0.1\gamma_d$ as the condition for the weak probe field approximation. Using the relevant parameters provided below, this condition gives the amplitude of the weak probe field an upper bound value of $\sim$1 V/m.

C. The refractive index of the atom gas due to atomic coherence

The complex electric polarization and magnetization of a single atom are given by $p = d_{cd}\rho_{dc}e^{-i\omega_p t} + \text{c.c.}$ and $m = (\mu_{ac}\rho_{ca} + \mu_{bc}\rho_{cb})e^{-i\omega_p t} + \text{c.c.}$, respectively. The positive frequency part of the electric polarization relates to the positive frequency part of the probe electric field as

$$d_{cd}\rho_{dc} = \alpha_e\epsilon_0\xi_E/2, \quad (5)$$

where α_e is the electric susceptibility of an atom and ϵ_0 is the dielectric constant of vacuum. Similarly, for the magnetic polarization, the relation is given by

$$\mu_0(\mu_{ac}\rho_{ca} + \mu_{bc}\rho_{cb}) = \alpha_m\xi_B/2, \quad (6)$$

where α_m is the magnetic susceptibility of an atom and μ_0 is the susceptibility of vacuum. On substituting Eq. (4) into this formula, the corresponding linear response coefficients are given by

$$\alpha_e = -\frac{i|d_{cd}|^2}{\hbar\epsilon_0(i\Delta_{dc}+\gamma_{dc})}\left[\frac{r_p}{\gamma_d}\rho_{dd}^{(0)} - \frac{r_p}{\gamma_c}\rho_{cc}^{(0)}\right], \tag{7}$$

$$\begin{aligned}\frac{\alpha_m}{\mu_0} = \frac{i}{\hbar}\Bigg\{ &- \frac{|\mu_{ca}|^2}{(i\Delta_{ca}+\gamma_{ca})}\left[\frac{r_p}{\gamma_c}\rho_{cc}^{(0)} - \frac{r_p}{\gamma_a}\rho_{aa}^{(0)}\right] \\ &+ \frac{|\mu_{ac}||\mu_{cb}|e^{i(\varphi_2-\varphi_1)}}{(i\Delta_{ca}+\gamma_{ca})}\frac{r_p\rho_{ba}^{(0)}}{(i\omega_{ba}+\gamma_{ba})}\Bigg\} \\ &+ \frac{i}{\hbar}\Bigg\{-\frac{|\mu_{cb}|^2}{(i\Delta_{cb}+\gamma_{cb})}\left[\frac{r_p}{\gamma_c}\rho_{cc}^{(0)} - \frac{r_p}{\gamma_b}\rho_{bb}^{(0)}\right] \\ &+ \frac{|\mu_{ca}||\mu_{bc}|e^{i(\varphi_1-\varphi_2)}}{(i\Delta_{cb}+\gamma_{cb})}\frac{r_p\rho_{ab}^{(0)}}{(\gamma_{ba}-i\omega_{ba})}\Bigg\}.\end{aligned} \tag{8}$$

As can be seen from the above equations, the phases of the Rabi frequencies can be absorbed into the phase of $\rho_{ab}^{(0)}$. Without loss of generality, we may choose $\varphi_1 - \varphi_2 = 0$.

According to the Clausius-Mossotti relations, by taking into account the local field effect in dense medium [35], the complex-valued relative permittivity and relative permeability of the atomic gas are given by

$$\epsilon = \epsilon_r + i\epsilon_i = \frac{1+\frac{2}{3}N\alpha_e}{1-\frac{1}{3}N\alpha_e}, \tag{9}$$

$$\mu = \mu_r + i\mu_i = \frac{1+\frac{2}{3}N\alpha_m}{1-\frac{1}{3}N\alpha_m}, \tag{10}$$

where N is the density of atoms and ϵ_r (μ_r) and ϵ_i (μ_i) are the real and imaginary parts of the permittivity (permeability), respectively. To see the effect of local field, we obtain the expression of μ_r and μ_i as

$$\mu_r = \frac{1+\frac{1}{3}\mathrm{Re}[N\alpha_m] - \frac{2}{9}|N\alpha_m|^2}{\left(1-\frac{1}{3}\mathrm{Re}[N\alpha_m]\right)^2 + \left(\frac{1}{3}\mathrm{Im}[N\alpha_m]\right)^2}, \tag{11}$$

$$\mu_i = \frac{\mathrm{Im}[N\alpha_m]}{\left(1-\frac{1}{3}\mathrm{Re}[N\alpha_m]\right)^2 + \left(\frac{1}{3}\mathrm{Im}[N\alpha_m]\right)^2}. \tag{12}$$

It is clear from the above equations that $1+\frac{1}{3}\mathrm{Re}[N\alpha_m] - \frac{2}{9}|N\alpha_m|^2 < 0$ is the condition of generating negative permeability. For a moderate value of atomic density, $\mathrm{Re}[N\alpha_m] < 0$ and $|N\alpha_m| > 1$ is required to realize negative μ_r. As can be seen from Eq. (8), a negative real part of magnetic susceptibility can be realized via the initial atomic coherence with proper phases.

For real relative permittivity and relative permeability, the negative refraction $n = -\sqrt{\epsilon_r\mu_r}$ when both $\epsilon_r < 0$ and $\mu_r < 0$ [1]. In general, for complex-valued ϵ and μ, the real part and the imaginary part of the refractive index are expressed as [36]

$$n_r = -\frac{1}{\sqrt{2}}\sqrt{|\epsilon||\mu| + \mu_r\epsilon_r - \mu_i\epsilon_i}, \tag{13}$$

$$n_i = -\frac{1}{\sqrt{2}}\frac{\mu_i\epsilon_r + \mu_r\epsilon_i}{\sqrt{|\epsilon||\mu| + \mu_r\epsilon_r - \mu_i\epsilon_i}}. \tag{14}$$

To show negative refractive index, the condition $\epsilon_r|\mu| + \mu_r|\epsilon| < 0$ should be satisfied [36]. To get nonabsorption, i.e., $n_i = 0$, the special case considered in Ref. [1] is set $\epsilon_i = 0$ and $\mu_i = 0$. For a general case, we have the condition $\mu_i\epsilon_r + \mu_r\epsilon_i = 0$ or $\mu_i/\epsilon_i = -\mu_r/\epsilon_r$. Since $\mu_r < 0$ and $\epsilon_r < 0$ for negative refraction, the ratio $\mu_i/\epsilon_i < 0$. This means that the magnetic component of the probe field is amplified while the electrical field is absorbed or vice versa. In the limit under consideration, $\epsilon_i \approx 1/|N\alpha_e|$, absorption of the magnetic field must be greatly depressed and the very small amount of gain must be created for the generation of negative refraction without absorption. In the following, we will show that this situation can be realized via quantum coherence and destructive quantum interference.

III. RESULTS AND DISCUSSIONS

In this section, we present numerical results to show negative refraction with zero absorption in the dense atom gas studied above. In particular, we consider the density of the atoms to be large enough such that $|N\alpha_e| \gg 1$. We then have $\epsilon_r \approx -2$ and the electric loss term $\epsilon_i \sim 1/N$ according to the Clausius-Mossotti relation [35]. For the magnetic component of the probe field, we show that negative μ_r as well as zero μ_i can be controlled via the atomic coherence [31]. Since the relative permittivity is largely unaffected due to the dense atoms, we focus on how to tune the relative permeability with a wide range of parameters.

A. Negative refraction with zero absorption

First, we consider an atomic density of 8×10^{17} cm^{-3}. The decay rates are $\gamma_a = \gamma_b = 2\gamma$, $\gamma_d = 5\gamma$, and $\gamma_c = 0.1\gamma$, where the typical value of γ is taken to be 10^7 Hz. The magnetic dipole moments are chosen have the relation $|\mu_{ca}| = |\mu_{cb}| = \mu_m$, where $\mu_m = c\sqrt{3\hbar\epsilon_0\gamma_B\lambda^3/8\pi^2}$. The electric dipole moment $|d_{dc}| = \sqrt{3\hbar\epsilon_0\gamma_E\lambda^3/8\pi^2}$. Here λ is the wavelength of the probe field which is taken to be 5 μm. The spontaneous emission rates γ_E and γ_B of levels $|d\rangle$ and $|c\rangle$ are chosen the typical values of 0.1γ and $0.1/(137)^2\gamma$, respectively. In Eqs. (8), all the detuning parameters can be written in the forms $\Delta_{ca} = \Delta + \omega_{ba}/2$ and $\Delta_{cb} = \Delta - \omega_{ba}/2$ by defining the detuning $\Delta = (\Delta_{cb} + \Delta_{ca})/2$, and the doublet spacing $\hbar\omega_{ba}$ is set to be $\hbar\gamma_{ba}$, which can be adjusted by use of a static magnetic field.

We initially pump the atoms with a rate of $r_p = 2\gamma$ with populations $\rho_{dd}^{(0)} = 0, \rho_{cc}^{(0)} = 0.01$, $\rho_{aa}^{(0)} = \rho_{bb}^{(0)} = |\rho_{ab}^{(0)}| = (1 - \rho_{dd}^{(0)} - \rho_{cc}^{(0)})/2$, and $\rho_{ab}^{(0)} = |\rho_{ba}|e^{i\pi/2}$.

In Figs. 2 and 3, we plot the electric susceptibility, the magnetic susceptibility, the relative permittivity, and the relative permeability of the atomic gas described above. The electric susceptibility curves are due to the interaction of the probe field with two-level atoms. The magnetic susceptibility curves are due to the interaction of the probe field with coherent prepared three-level atoms [37] which cancels the absorption. With the large density of atoms, the local field effect dominates, and therefore we have $\epsilon_r \approx -2$ and $\epsilon_i \approx 0$. For the relative permeability, the curves shown in Fig. 3(b) are the overall effects of the local field of the dense atoms and quantum interference of the coherent states.

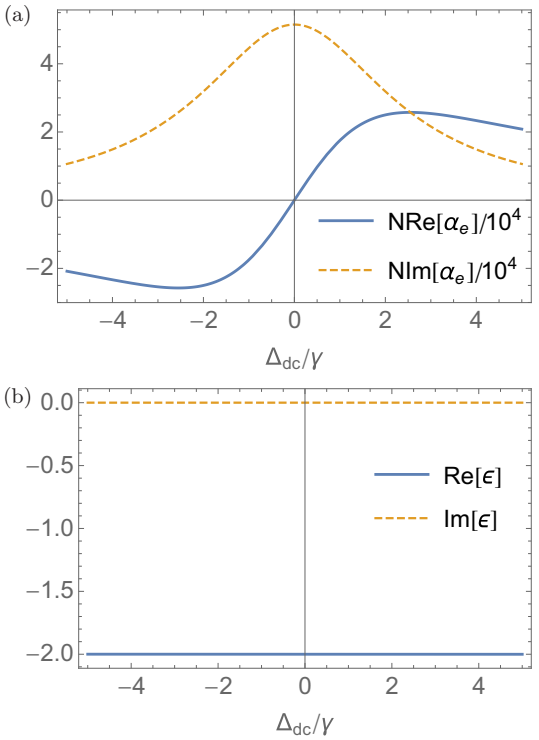

FIG. 2. (a) Real part (solid curve) and imaginary part (dashed curve) of the electric susceptibility. (b) Real part (solid curve) and imaginary part (dashed curve) of the relative permittivity.

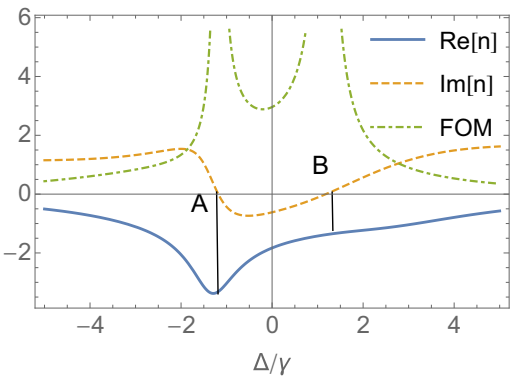

FIG. 4. Real part (solid curve) and imaginary part (dashed curve) of the refractive index, and FOM (dot-dashed curve) with the parameters in Fig. 2.

In Fig. 4, we plot both the real part and the imaginary part of the refractive index of the atoms according the Eqs. (13) and (14). We find that negative refraction can be achieved in a wide range of detuning with small absorption. Moreover, there are two values of detuning with zero absorption (at points A and B in the figure) which is due to the quantum interference of the atomic coherence [31]. To see how well the performance of the atom gas for negative refraction, we also plot a curve of FOM. We observe that there are two windows of FOM $\gg 1$ located around the zero-absorption detunings.

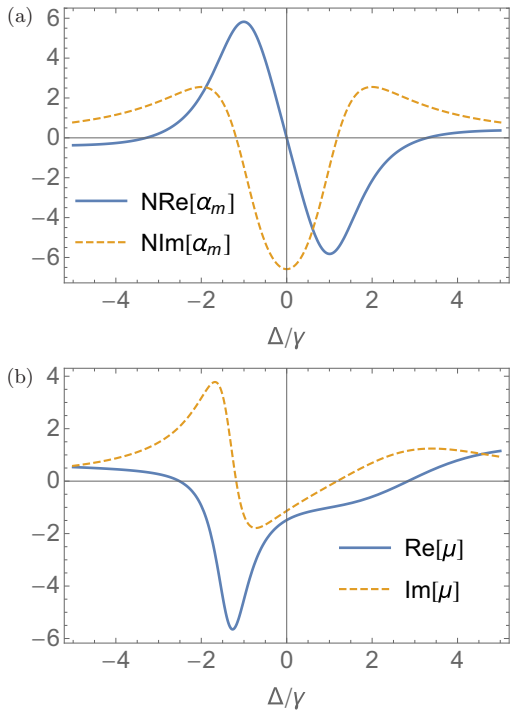

FIG. 3. (a) Real part (solid curve) and imaginary part (dashed curve) of the magnetic susceptibility. (b) Real part (solid curve) and imaginary part (dashed curve) of the relative permeability.

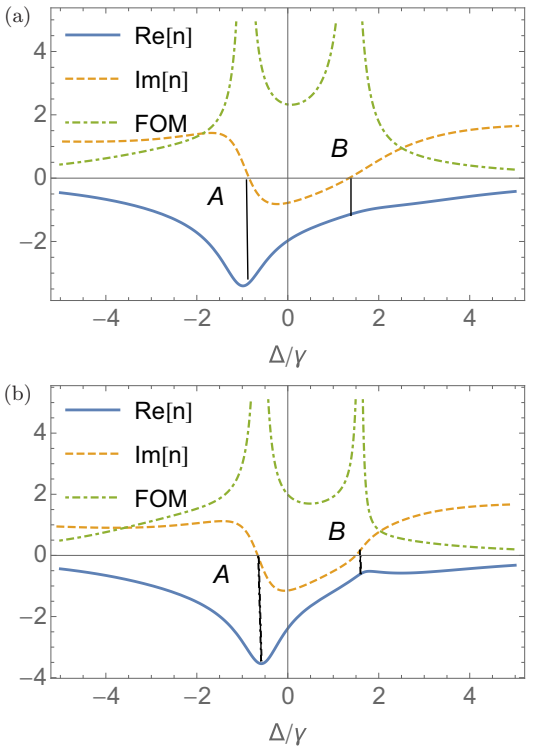

FIG. 5. (a) Real part (solid curve), imaginary part (dashed curve), and FOM (dot-dashed curve) of the refractive index for $|\mu_{cb}| = 0.8\mu_m$. (b) Real part (solid curve), imaginary part (dashed curve), and FOM (dot-dashed curve) of the refractive index for $|\mu_{cb}| = 0.6\mu_m$. The other parameters are the same as in Fig. 2.

B. Unequal magnetic dipole moments

For a real atomic gas, the magnetic dipole moments of the two transitions may not be the same. Therefore, we study the effect of the unequal dipole moments. We take $|\mu_{ca}| = \mu_m$ and vary the value of $|\mu_{cb}|$.

In Fig. 5, we plot the curves of the relative permeabilities and the refractive indexes for two different values of $|\mu_{cb}| = 0.8\mu_m$ and $|\mu_{cb}| = 0.6\mu_m$. We observe that negative refraction and zero absorption can be achieved even if $|\mu_{ca}| \neq \mu_{cb}$. As a comparison to Fig. 4, we see that with increasing unequal dipole moments that the left position of the zero absorption window (point A) is shifted closer to the center while the right position of the zero absorption window (point B) is shifted away from the center. The solutions of $\mathrm{Im}[N\alpha_m] = 0$ are determined by the values of $|\mu_{cb}|$ and $|\mu_{ca}|$ from Eq. (8). Therefore, the solutions of $n_i = 0$ are the same as those of $\mathrm{Im}[N\alpha_m] = 0$ ($\epsilon_i = 0$ is considered in the large density limit) from Eqs. (12) and (14), which depend on the values of $|\mu_{cb}|$ and $|\mu_{ca}|$.

C. Effects of the atomic decay rates

We consider the effects when we change the decay rates from the doublet levels $|a\rangle$ and $|b\rangle$. We use the same parameters as in Sec. III A except that γ_a and γ_b. We plot the results of the refractive indexes for $\gamma_a = \gamma_b = 2.5\gamma$ and $\gamma_a = \gamma_b = 1.25\gamma$.

In Fig. 6, the separation of the two zero-absorption windows is increased with larger decay rates as can be seen from points A and B. It can also be observed from the curves of FOM that the width of each window increases with increasing decay rates. Therefore, our theoretical model works well with different possible decay rates.

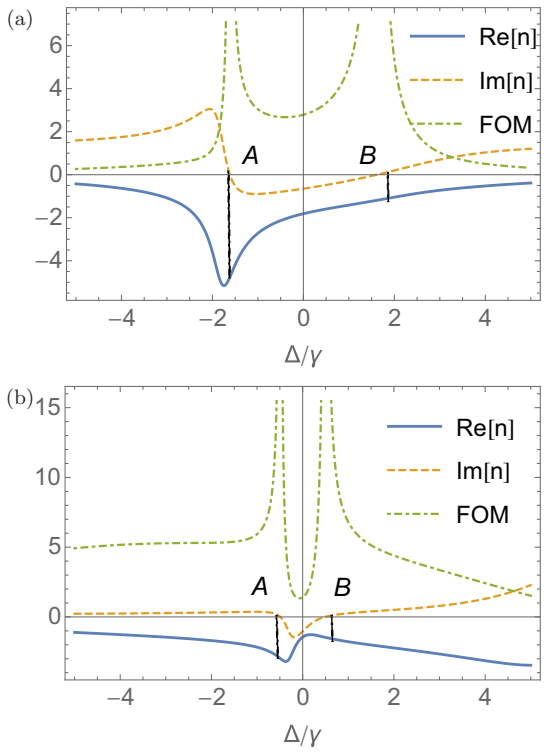

FIG. 6. (a) Real part (solid curve), imaginary part (dashed curve), and FOM (dot-dashed curve) of the refractive index for $\gamma_a = \gamma_b = 2.5\gamma$. (b) Real part (solid curve), imaginary part (dashed curve), and FOM (dot-dashed curve) of the refractive index for $\gamma_a = \gamma_b = 1.25\gamma$. The other parameters are the same as in Fig. 2.

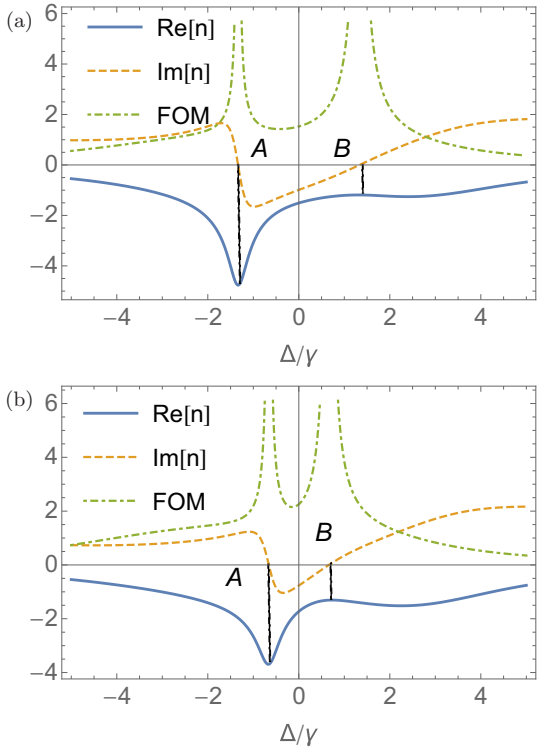

FIG. 7. (a) Real part (solid curve), imaginary part (dashed curve), and FOM (dot-dashed curve) of the refractive index for $\omega_{ab} = 3\gamma$. (b) Real part (solid curve), imaginary part (dashed curve), and FOM (dot-dashed curve) of the refractive index for $\omega_{ab} = \gamma$. The other parameters are the same as in Fig. 2.

D. Effects of the doublet splitting

We study the effects of the doublet splitting on the preparation of negative refractive index by varying the value of the doublet splitting ω_{ab}. We consider two different values of $\omega_{ab} = 3\gamma$ and $\omega_{ab} = \gamma$ as shown in Fig. 7. It can be seen from the curves that negative refraction with zero absorption is feasible with different values of ω_{ab}. As a comparison with Fig. 4, we see that smaller ω_{ab} results in smaller separation between two zero-absorption windows. Therefore, by controlling the doublet splitting, we can tune the refractive index as well as control the positions of detuning for zero absorption (points A and B) of the atomic gas.

E. Effects of the atomic coherence

Now we examine the effects of the atomic coherence on the negative refractive index and FOM. We consider the atomic coherence with different phases and different populations for illustrations. Specifically, we consider two cases: One with $\rho_{ab}^{(0)} = |\rho_{ab}^{(0)}|e^{i5\pi/4}$ and the other one with $\rho_{cc}^{(0)} = 0.015$ and $\rho_{aa}^{(0)} = \rho_{bb}^{(0)} = |\rho_{ab}^{(0)}| = 0.4925$. The other parameters are the same as given in Sec. III A.

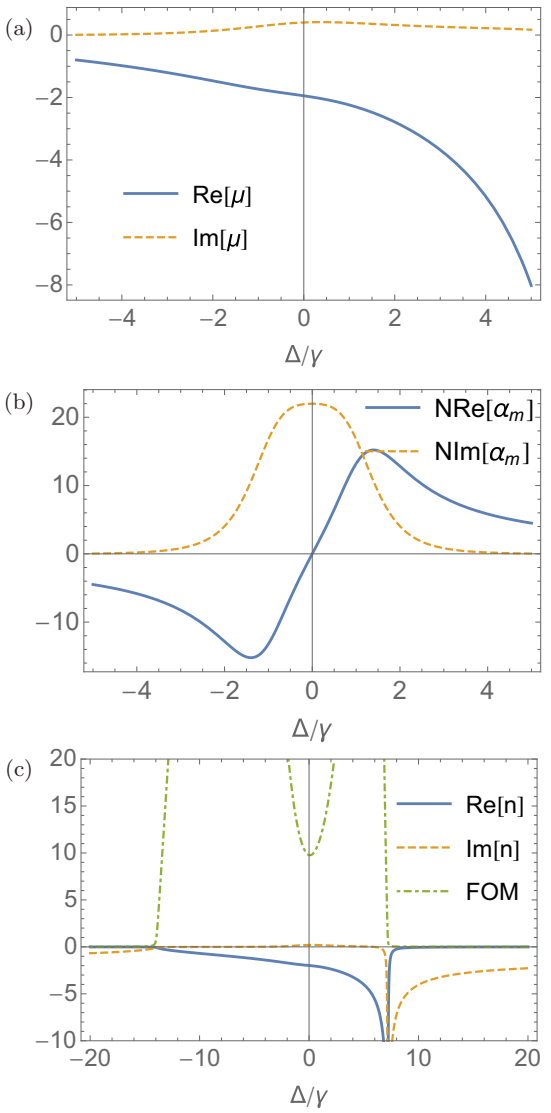

FIG. 8. Real part (solid curve) and imaginary part (dashed curve) of (a) the relative permeability; (b) the magnetic susceptibility; (c) the refractive index. $\rho_{ab}^{(0)} = |\rho_{ab}^{(0)}|e^{i5\pi/4}$. The other parameters are the same as in Fig. 2.

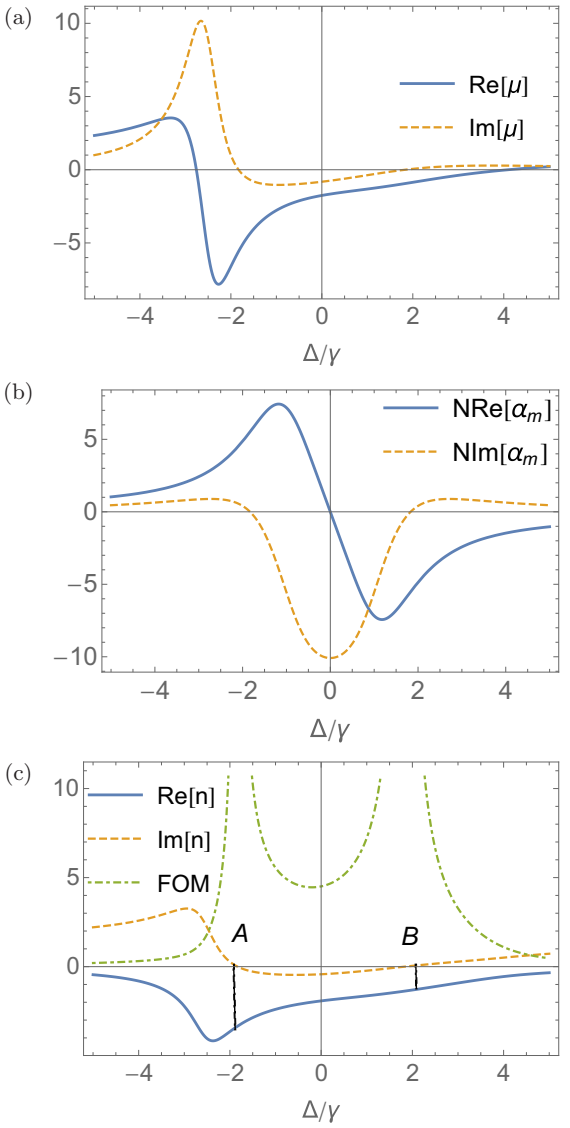

FIG. 9. Real part (solid curve) and imaginary part (dashed curve) of (a) the relative permeability; (b) the magnetic susceptibility; (c) the refractive index. $\rho_{aa}^{(0)} = \rho_{bb}^{(0)} = |\rho_{ab}^{(0)}| = 0.4925$ and $\rho_{cc}^{(0)} = 0.015$. The other parameters are the same as in Fig. 2.

In the first case, when the phase between the atomic levels $|a\rangle$ and $|b\rangle$ is changed, we see from Fig. 8(a) that $\mu_r < 0$ and $\mu_i \approx 0$ are achieved simultaneously for a wider range of detunings compared with Fig. 3. This is due to the fact that either $|\mathrm{Re}[N\alpha_m]|$ or $|\mathrm{Im}[N\alpha_m]|$ is much greater than 1 for a wide range of detuning as shown in Fig. 8(b). In this case, although strong absorption happens due to the atomic coherence for a single atom, the relative permeability can be negative by taking into account the local field effect. Therefore, we obtain a wide window of zero absorption for negative refraction by tuning the phase of the atomic coherence [see Fig. 8(c)].

In the other case, when the population on level $|c\rangle$ is slightly changed, we observe that a wider zero-absorption window (see Fig. 9(c) points A and B) is obtained compared to the case in Fig. 4. We also plot the magnetic susceptibility in Fig. 9(b). It is shown that stronger emission compared to that in Fig. 2 is obtained due to the increase of the population on the excited atomic level $|c\rangle$.

Therefore, we find the refractive index is very sensitive to the atomic coherence since $\mathrm{Re}[N\alpha_m]$ and $\mathrm{Im}[N\alpha_m]$ can be modified greatly by even a slight change on the atomic coherence. This can be used to control the negative refraction and minimize the absorption of the probe field.

Moreover, if fixing all the parameters except with the phase of the initial atomic coherence state, the maximum negative real part of the permeability can be obtained by optimizing the phase of the atomic state. This is done by maximizing figure of merit with a large real part but a small imaginary part of the refractive index.

F. Effects of the atomic density

In this subsection, we show that the negative refraction as well as zero absorption can be realized with a wide range of

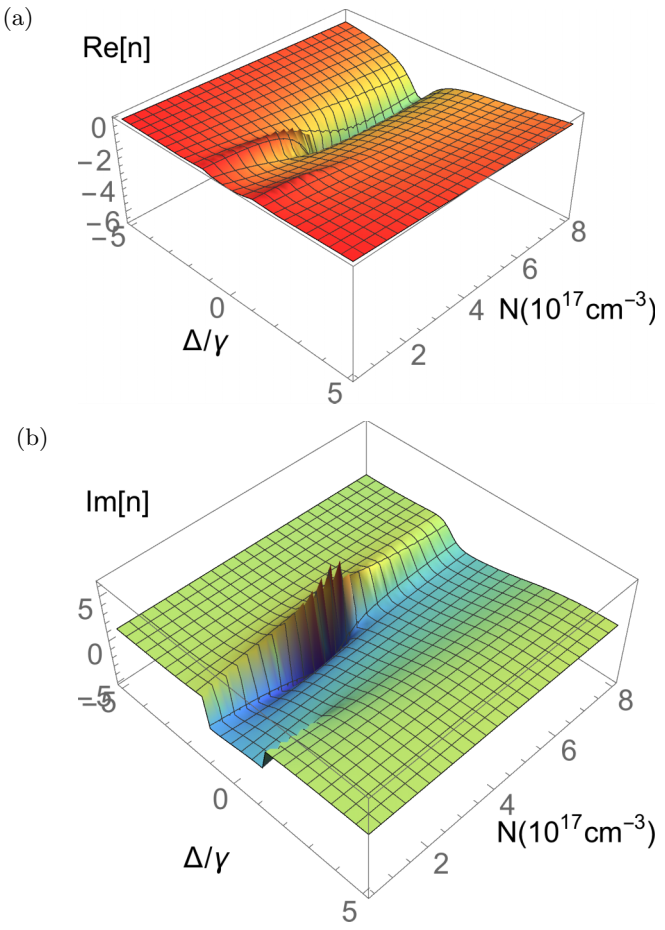

FIG. 10. (a) Real part and (b) imaginary part of the refractive index against the atomic density and detuning. The other parameters are the same as in Fig. 2.

atomic densities. As can be seen from Eqs. (11) and (12), for large N such that $|N\alpha_m| \gg 1$, the local field effect becomes dominant. While for smaller N such that $|N\alpha_m| \sim 1$ the overall effect of the local field and the atomic coherence determines the refractive index of the atom gas.

In Fig. 10, we plot the real part and the imaginary part of the refractive index as a function of the atomic density N and the detuning Δ/γ. We observe that negative refraction is possible with different atomic densities. Zero value even negative values of the imaginary part of the refractive index can be achieved by exploiting the atomic coherence. Around the parameters of zero imaginary part and negative real part, very large FOM can be obtained which makes the atom gas a good candidate for left-hand side materials.

Similarly, since $N\alpha_e$, $N\alpha_m \propto N, r_p$, the same effect of the atomic density N applies to that of the pumping rate r_p.

G. Possible experimental realization

It may be challenge to find the exact four-level scheme as shown in Fig. 1 which has neighboring magnetic dipole transition and electric dipole transition with similar spacing in the range of infrared wavelengths. However, a revised five-level scheme in metastable neon gas as shown in Fig. 11 may be suitable for experimental realization. According to Eq. (7),

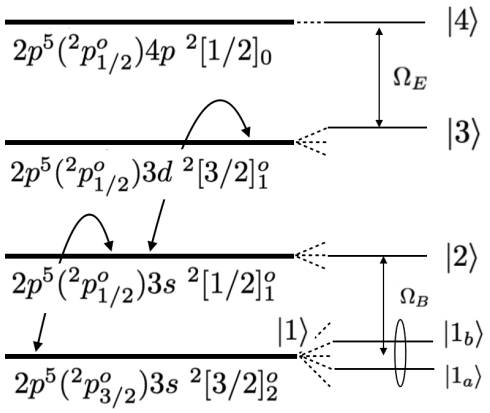

FIG. 11. Five-level scheme in neon gas with Zeeman splittings [38].

the linear responses of the electric field and the magnetic field are independent of each other and the weak probe field does not alter the initial population on the atomic levels. Therefore, the electric dipole transition and the magnetic dipole transition are not required to be next to each other, as is in the case of the five-level scheme in metastable neon gas. In Fig. 11, the electric transition $|3\rangle \rightarrow |4\rangle$ and the magnetic transition $|1\rangle \rightarrow |2\rangle$ are in the infrared range at a wavelength around 5 μm. A static magnetic field is applied to the atomic gas to split the ground state $|1\rangle$ into $|1_a\rangle$ and $|1_b\rangle$. Two strong incoherent pumping beams are used to create steady-state population on levels $|2\rangle$ and $|3\rangle$ to mimic the results in Eq. (4). Therefore, negative refraction without absorption via quantum coherence may be feasible with the revised scheme in Fig. 11.

IV. CONCLUSION

In conclusion, we have proposed a novel scheme for the realization of negative refraction with zero absorption in an atomic gas consisting of cascade-type four-level atoms via atomic coherence. Zero absorption is achieved by using quantum inference of the initially prepared atomic coherence.

We exploited the master equation to obtain the steady-state solution of the response of the atoms in the presence of a weak probe field. We derived analytical expressions of both the electric permittivity and the magnetic permeability by taking into account of the local field effect. The real parts of the electric permittivity and the magnetic permeability of the atomic gas can be made negative simultaneously to achieve negative refraction. Vanishing imaginary part of the electric permittivity is obtained due to the local field effect of the dense atoms according to Clausius-Mossotti relation. Vanishing imaginary part of the magnetic permeability is obtained due to absorption cancellation in the presence of the atomic coherence. We studied a wide range of parameters of the atomic gas to show negative refraction. We also discussed a possible scheme for experimental realization.

ACKNOWLEDGMENTS

This research of A.P.F., M.W., and F.L.L. was supported by the National Natural Science Foundation of China under Grants No. 11374239 and No. 11534008. The research of

W.G. and M.S.Z. is supported by NPRP Grant No. 7-210-1-032 by the Qatar National Research Fund (QNRF).

APPENDIX: FULL MASTER EQUATION

In this Appendix, we first obtain the full master equation by considering all orders of the probe field and then we derive the steady-state solution Eq. (4) in the main article under the approximation $\Omega_{B1},\Omega_{B2},\Omega_E \ll \gamma_j,r_p,\Delta_{ij}(i,j=a,b,c,d.)$.

According to the master equation, the complete equations of each matrix element are given by

$$\dot{\rho}_{aa} = -\gamma_a\rho_{aa} + r_p\rho_{aa}^{(0)} + i\frac{\Omega_{B1}}{2}(e^{-i\varphi_1}\rho_{ca} - \text{H.c.}), \quad \text{(A1)}$$

$$\dot{\rho}_{bb} = -\gamma_b\rho_{bb} + r_p\rho_{bb}^{(0)} + i\frac{\Omega_{B2}}{2}(e^{-i\varphi_2}\rho_{cb} - \text{H.c.}), \quad \text{(A2)}$$

$$\dot{\rho}_{cc} = -\gamma_c\rho_{cc} + r_p\rho_{cc}^{(0)} - i\frac{\Omega_{B1}}{2}(e^{-i\varphi_1}\rho_{ca} - \text{H.c.}) - i\frac{\Omega_{B2}}{2}(e^{-i\varphi_2}\rho_{cb} - \text{H.c.}) - \text{i}\frac{\Omega_{\text{E}}}{2}(\text{e}^{\text{i}\varphi_3}\rho_{\text{cd}} - \text{H.c.}), \quad \text{(A3)}$$

$$\dot{\rho}_{dd} = -\gamma_d\rho_{dd} + r_p\rho_{dd}^{(0)} + i\frac{\Omega_E}{2}(e^{i\varphi_3}\rho_{cd} - \text{H.c.}), \quad \text{(A4)}$$

$$\dot{\rho}_{ca} = -(i\Delta_{ca} + \gamma_{ca})\rho_{ca} + i\frac{\Omega_{B1}}{2}e^{i\varphi_1}(\rho_{aa} - \rho_{cc}) + i\frac{\Omega_{B2}}{2}e^{i\varphi_2}\rho_{ba} + i\frac{\Omega_E}{2}e^{-i\varphi_3}\rho_{da}, \quad \text{(A5)}$$

$$\dot{\rho}_{cb} = -(i\Delta_{cb} + \gamma_{cb})\rho_{cb} + i\frac{\Omega_{B2}}{2}e^{i\varphi_2}(\rho_{bb} - \rho_{cc}) + i\frac{\Omega_{B1}}{2}e^{i\varphi_1}\rho_{ab} + i\frac{\Omega_E}{2}e^{-i\varphi_3}\rho_{db}, \quad \text{(A6)}$$

$$\dot{\rho}_{dc} = -(i\Delta_{dc} + \gamma_{dc})\rho_{dc} + i\frac{\Omega_E}{2}e^{i\varphi_3}(\rho_{cc} - \rho_{dd}) - i\frac{\Omega_{B1}}{2}e^{-i\varphi_1}\rho_{da} - i\frac{\Omega_{B2}}{2}e^{-i\varphi_2}\rho_{db}, \quad \text{(A7)}$$

$$\dot{\rho}_{da} = -(i\Delta_{dc} + i\Delta_{ca} + \gamma_{da})\rho_{da} + i\frac{\Omega_E}{2}e^{i\varphi_3}\rho_{ca} - i\frac{\Omega_{B1}}{2}e^{i\varphi_1}\rho_{dc}, \quad \text{(A8)}$$

$$\dot{\rho}_{db} = -(i\Delta_{dc} + i\Delta_{cb} + \gamma_{db})\rho_{db} + i\frac{\Omega_E}{2}e^{i\varphi_3}\rho_{cb} - i\frac{\Omega_{B2}}{2}e^{i\varphi_2}\rho_{dc}, \quad \text{(A9)}$$

$$\dot{\rho}_{ab} = (i\omega_{ba} - \gamma_{ba})\rho_{ab} + r_p\rho_{ab}^{(0)} - i\frac{\Omega_{B2}}{2}e^{i\varphi_2}\rho_{ac} + i\frac{\Omega_{B1}}{2}e^{-i\varphi_1}\rho_{cb}. \quad \text{(A10)}$$

On solving Eqs. (A8)–(A10), we obtain the steady-state results for ρ_{da}, ρ_{db}, and ρ_{ab} as

$$\rho_{da} = \frac{i\Omega_E e^{i\varphi_3}\rho_{ca}/2}{i\Delta_{dc} + i\Delta_{ca} + \gamma_{da}} - \frac{i\Omega_{B1}e^{i\varphi_1}\rho_{dc}/2}{i\Delta_{dc} + i\Delta_{ca} + \gamma_{da}}, \quad \text{(A11)}$$

$$\rho_{db} = \frac{i\Omega_E e^{i\varphi_3}\rho_{cb}/2}{i\Delta_{dc} + i\Delta_{cb} + \gamma_{db}} - \frac{i\Omega_{B2}e^{i\varphi_2}\rho_{dc}/2}{i\Delta_{dc} + i\Delta_{cb} + \gamma_{db}}, \quad \text{(A12)}$$

$$\rho_{ab} = \frac{r_p}{\gamma_{ba} - i\omega_{ba}}\rho_{ab}^{(0)} - \frac{i\Omega_{B2}e^{i\varphi_2}/2}{\gamma_{ba} - i\omega_{ba}}\rho_{ac} + \frac{i\Omega_{B1}e^{-i\varphi_1}/2}{\gamma_{ba} - i\omega_{ba}}\rho_{cb}. \quad \text{(A13)}$$

On substituting ρ_{da}, ρ_{db} and ρ_{ab} into Eqs. (A5)–(A7), we obtain a set of equations for ρ_{ca}, ρ_{cb}, and ρ_{dc} at the steady state.

$$A_1\rho_{ca} = B_1\rho_{bc} + C_1\rho_{dc} + D_1, \quad \text{(A14)}$$

$$A_2\rho_{cb} = B_2\rho_{ac} + C_2\rho_{dc} + D_2, \quad \text{(A15)}$$

$$A_3\rho_{dc} = B_3\rho_{ca} + C_3\rho_{cb} + D_3, \quad \text{(A16)}$$

where the coefficients A_j,B_j,C_j,D_j are given by

$$A_1 = \gamma_{ca} - i\Delta_{ca} + \frac{\Omega_{B2}^2/4}{\gamma_{ba} + i\omega_{ba}} + \frac{\Omega_E^2/4}{\gamma_{da} + i\Delta_{dc} + i\Delta_{ca}},$$

$$A_2 = \gamma_{cb} + i\Delta_{cb} + \frac{\Omega_{B1}^2/4}{\gamma_{ba} - i\omega_{ba}} + \frac{\Omega_E^2/4}{\gamma_{db} + i\Delta_{dc} + i\Delta_{cb}},$$

$$A_3 = \gamma_{dc} + i\Delta_{dc} + \frac{\Omega_{B1}^2/4}{\gamma_{da} + i\Delta_{dc} + i\Delta_{ca}} + \frac{\Omega_{B2}^2/4}{\gamma_{db} + i\Delta_{dc} + i\Delta_{cb}},$$

$$B_1 = \frac{\Omega_{B1}\Omega_{B2}e^{i(\varphi_1+\varphi_2)}/4}{\gamma_{ba} + i\omega_{ba}}, \quad B_2 = \frac{\Omega_{B1}\Omega_{B2}e^{i(\varphi_1+\varphi_2)}/4}{\gamma_{ba} - i\omega_{ba}},$$

$$B_3 = \frac{\Omega_E\Omega_{B1}e^{i(\varphi_3-\varphi_1)}/4}{\gamma_{da} + i\Delta_{dc} + i\Delta_{ca}}, \quad C_1 = \frac{\Omega_E\Omega_{B1}e^{i(\varphi_1-\varphi_3)}/4}{\gamma_{da} + i\Delta_{dc} + i\Delta_{ca}},$$

$$C_2 = \frac{\Omega_E\Omega_{B2}e^{i(\varphi_2-\varphi_3)}/4}{\gamma_{db} + i\Delta_{dc} + i\Delta_{cb}}, \quad C_3 = \frac{\Omega_E\Omega_{B2}e^{i(\varphi_3-\varphi_2)}/4}{\gamma_{db} + i\Delta_{dc} + i\Delta_{cb}},$$

$$D_1 = i\frac{\Omega_{B1}e^{i\varphi_1}}{2}(\rho_{aa} - \rho_{cc}) + i\frac{\Omega_{B2}e^{i\varphi_2}r_p/2}{\gamma_{ba} + i\omega_{ba}}\rho_{ba}^{(0)},$$

$$D_2 = i\frac{\Omega_{B2}e^{i\varphi_2}}{2}(\rho_{bb} - \rho_{cc}) + i\frac{\Omega_{B1}e^{i\varphi_1}r_p/2}{\gamma_{ba} - i\omega_{ba}}\rho_{ab}^{(0)},$$

$$D_3 = i\frac{\Omega_E e^{i\varphi_3}}{2}(\rho_{cc} - \rho_{dd}). \quad \text{(A17)}$$

On solving Eq. (A16) and substituting the result of ρ_{dc} into Eqs. (A14) and (A15), we obtain

$$\left(A_1 - \frac{B_3C_1}{A_3}\right)\rho_{ca} = B_1\rho_{bc} + \frac{C_3C_1}{A_3}\rho_{cb} + D_1 + \frac{D_3C_1}{A_3}, \quad \text{(A18)}$$

$$\left(A_2 - \frac{C_3C_2}{A_3}\right)\rho_{cb} = B_2\rho_{ac} + \frac{B_3C_2}{A_3}\rho_{ca} + D_2 + \frac{D_3C_2}{A_3}. \quad \text{(A19)}$$

Equations (A18) and (A19) are exact coupled equations between the matrix elements ρ_{ca} and ρ_{cb} at steady state. Using the relation Ω_{B1}, Ω_{B2}, $\Omega_E \ll \gamma_j,r_p$, and Δ_{ij}, we find that $\frac{C_3C_1}{A_3} \sim \frac{\Omega_E^2}{\gamma_d^2}B_1 \ll B_1$, $\frac{D_3C_1}{A_3} \sim \frac{\Omega_E^2}{\gamma_d^2}D_1 \ll D_1$, and $\frac{B_3C_1}{A_3} \sim \frac{\Omega_E^2\Omega_{B1}^2}{\gamma_d^3} \ll A_1$. Similarly, $\frac{B_3C_2}{A_3} \ll B_2$, $\frac{D_3C_2}{A_3} \ll D_2$, and $\frac{C_3C_2}{A_3} \ll A_2$. Although the electric Rabi frequency, Ω_E, is two orders

larger than the magnetic Rabi frequencies, Ω_{B1},Ω_{B2}, the magnetic dipole contribution that comes from the electric coupling is negligible. Furthermore, since $B_j \ll A_j$, we can neglect the coupling between the off-diagonal matrix elements ρ_{ca}, ρ_{cb}, and ρ_{dc}. Therefore, the solutions of Eqs. (A14)–(A16) are given by

$$\rho_{ca} = \frac{D_1}{A_1}, \quad \rho_{cb} = \frac{D_2}{A_2}, \quad \rho_{dc} = \frac{D_3}{A_3}. \tag{A20}$$

The above results show that up to the first order in Ω_E, Ω_{B_1},Ω_{B_2}, there is no chirality in this scheme. On substituting the results in the Eq. (A20) into the Eqs. (A1)–(A4) and keeping up the first order in Ω_{B1}, Ω_{B2}, Ω_E, we obtain the results of the diagonal matrix elements at the steady state as

$$\rho_{aa} \approx \frac{r_p \rho_{aa}^{(0)}}{\gamma_a}, \quad \rho_{bb} \approx \frac{r_p \rho_{bb}^{(0)}}{\gamma_b},$$
$$\rho_{dd} \approx \frac{r_p \rho_{dd}^{(0)}}{\gamma_d}, \quad \rho_{cc} \approx \frac{r_p \rho_{cc}^{(0)}}{\gamma_c}. \tag{A21}$$

On substituting these results into the Eq. (A20) and keeping up to the first order in Ω_{B1}, Ω_{B2}, Ω_E, we obtain the results of the off-diagonal matrix elements at the steady state in Eq. (4).

[1] V. G. Veselago, Sov. Phys. Usp. **10**, 509 (1968).
[2] P. R. Berman, Phys. Rev. E **66**, 067603 (2002).
[3] M. W. Feise, P. J. Bevelacqua, and J. B. Schneider, Phys. Rev. B **66**, 035113 (2002).
[4] K. Aydin, I. Bulu, and E. Ozbay, Appl. Phys. Lett **90**, 254102 (2007).
[5] J. B. Pendry, Phys. Rev. Lett. **85**, 3966 (2000).
[6] D. R. Smith, W. J. Padilla, D. C. Vier, S. C. Nemat-Nasser, and S. Schultz, Phys. Rev. Lett. **84**, 4184 (2000).
[7] R. A. Shelby, D. R. Smith, and S. Schultz, Science **292**, 77 (2001).
[8] T. J. Yen, W. J. Padilla, N. Fang, D. C. Vier, D. R. Smith, J. B. Pendry, D. N. Basov, and X. Zhang, Science **303**, 1494 (2004).
[9] Stefan Linden, Christian Enkrich, Martin Wegener, Jiangfeng Zhou, Thomas Koschny, and C. M. Soukoulis, Science **306**, 1351 (2004).
[10] J. B. Pendry, Science **306**, 1353 (2004).
[11] C. Enkrich, M. Wegener, S. Linden, S. Burger, L. Zschiedrich, F. Schmidt, J. F. Zhou, Th. Koschny, and C. M. Soukoulis, Phys. Rev. Lett. **95**, 203901 (2005).
[12] A. Pimenov, P. Przyslupski, A. Loidl, and B. Dabrowski, Phys. Rev. Lett. **95**, 247009 (2005).
[13] E. Cubukcu, K. Aydin, E. Ozbay. S. Foteinopoulou, and C. M. Soukoulis, Nature (London) **423**, 604 (2003).
[14] Sailing He, Zhichao Ruan, Long Chen, and Jianqi Shen, Phys. Rev. B **70**, 115113 (2004).
[15] A. Berrier, M. Mulot, M. Swillo, M. Qiu, L. Thylen, A. Talneau, and S. Anand, Phys. Rev. Lett. **93**, 073902 (2004).
[16] David R. Smith, David Schurig, Marshall Rosenbluth, Sheldon Schultz, S. Anantha Ramakrishna, and John B. Pendry, Appl. Phys. Lett. **82**, 1506 (2003).
[17] V. P. Drachev, W. Cai, U. Chettiar, H.-K. Yuan, A. K. Sarychev, A. V. Kildishev, G. Klimeck, and V. M. Shalaev, Laser Phys. Lett. **3**, 49 (2006).
[18] Vladimir M. Shalaev, Nat. Photon. **1**, 41 (2007).
[19] G. Dolling, M. Wegener, C. M. Soukoulis, and S. Linden, Opt. Lett. **32**, 53 (2007).
[20] M. Ö. Oktel and Ö. E. Müstecaplioğlu, Phys. Rev. A **70**, 053806 (2004).
[21] Q. Thommen and P. Mandel, Phys. Rev. Lett. **96**, 053601 (2006).
[22] J. Kästel, M. Fleischhauer, S. F. Yelin, and R. L. Walsworth, Phys. Rev. Lett. **99**, 073602 (2007).
[23] Fu-li Li, Ai-ping Fang, and Meng Wang, J. Phys. B: At. Mol. Opt. Phys. **42**, 195505 (2009).
[24] D. E. Sikes and D. D. Yavuz, Phys. Rev. A **82**, 011806(R) (2010).
[25] Peter P. Orth, Roman Hennig, Christoph H. Keitel, and Jörg Evers, New J. Phys. **15**, 013027 (2013).
[26] Shuncai Zhao, Zhengdong Liu, and Qixuan Wu, J. Phys. B: At. Mol. Opt. Phys. **43**, 045505 (2010).
[27] Shun-Cai Zhao, Zheng-Dong Liu, and Qi-Xuan Wu, Opt. Comm. **283**, 3301 (2010).
[28] Huifang Zhang, Haihong Ren, Xiaona Yan, and Lihua Bai, J. Mod. Opt. **59**, 1133 (2012).
[29] J.-Q. Shen, Prog. Electromagn. Res. **133**, 37 (2013).
[30] Michael Fleischhauer, Atac Imamoglu, and Jonathan P. Marangos, Rev. Mod. Phys. **77**, 633 (2005).
[31] M. O. Scully, Phys. Rev. Lett. **67**, 1855 (1991).
[32] J. Mlynek and W. Lange, Opt. Commun. **30**, 337 (1979).
[33] M. Fleischhauer, C. H. Keitel, M. O. Scully, C. Su, B. T. Ulrich, and S. Y. Zhu, Phys. Rev. A **46**, 1468 (1992).
[34] M. Jain, H. Xia, G. Y. Yin, A. J. Merriam, and S. E. Harris, Phys. Rev. Lett. **77**, 4326 (1996).
[35] J. D. Jackson, *Classical Electrodynamics* (Wiley, New York, 1998).
[36] R. A. Depine and A. Lakhtakia, Microw. Opt. Technol. Lett. **41**, 315 (2004).
[37] M. O. Scully and M. S. Zubairy, *Quantum Optics* (Cambridge University Press, Cambridge, 1997).
[38] http://physica.nist.gov/PhysRefData